

NASA/CR-2000-210320
ICASE Report No. 2000-30



General Framework for Achieving Textbook Multigrid Efficiency: One-dimensional Euler Example

James L. Thomas
NASA Langley Research Center, Hampton, Virginia

Boris Diskin
ICASE, Hampton, Virginia

Achi Brandt
The Weizmann Institute of Science, Rehovot, Israel

Jerry C. South, Jr.
Williamsburg, Virginia

Institute for Computer Applications in Science and Engineering
NASA Langley Research Center, Hampton, VA
Operated by Universities Space Research Association



National Aeronautics and
Space Administration

Langley Research Center
Hampton, Virginia 23681-2199

Prepared for Langley Research Center
under Contract NAS1-97046

August 2000

DISTRIBUTION STATEMENT A
Approved for Public Release
Distribution Unlimited

20000907 089

GENERAL FRAMEWORK FOR ACHIEVING TEXTBOOK MULTIGRID EFFICIENCY: ONE-DIMENSIONAL EULER EXAMPLE

JAMES L. THOMAS*, BORIS DISKIN†, ACHI BRANDT‡, AND JERRY C. SOUTH, JR.§

Abstract. A general multigrid framework is discussed for obtaining textbook efficiency to solutions of the compressible Euler and Navier-Stokes equations in conservation law form. The general methodology relies on a distributed relaxation procedure to reduce errors in regular (smoothly varying) flow regions; separate and distinct treatments for each of the factors (elliptic and/or hyperbolic) are used to attain optimal reductions of errors. Near boundaries and discontinuities (shocks), additional local relaxations of the conservative equations are necessary. Example calculations are made for the quasi-one-dimensional Euler equations; the calculations illustrate the general procedure.

Key words. textbook multigrid efficiency, distributed relaxation, Euler equations

Subject classification. Applied and Numerical Mathematics

1. Introduction. Computational fluid dynamics (CFD) has become an integral part of the aircraft design cycle because of the availability of faster computers with more memory and improved numerical algorithms and physical models. More impact is possible if reliable methods can be devised for off-design performance, generally associated with unsteady, separated, vortical flows with strong shock waves. Such computations demand significantly more computing resources than are currently available.

The current Reynolds-averaged Navier-Stokes (RANS) solvers with multigrid algorithms require on the order of 1500 residual evaluations to converge the lift and drag to one percent of their final values, even for relatively simple wing-body geometries at transonic cruise conditions. It is well known for elliptic problems that solutions can be attained optimally by using a full multigrid (FMG) process in far fewer (on the order of 2 to 4) residual evaluations. A multigrid method is defined by Brandt [2, 3, 4] as having textbook multigrid efficiency (TME) if the solutions to the governing system of equations are attained in a computational work that is a small (less than 10) multiple of the operation count in the discretized system of equations. Thus, operation count may be reduced by several orders of magnitude if TME can be attained for the RANS equations.

State-of-the-art multigrid methodologies for large-scale compressible flow applications use a block-matrix relaxation and/or a pseudo-time-dependent approach to solve the equations; significant improvements have been demonstrated with multigrid approaches, but the methods are not optimally convergent. The RANS equation sets are systems of coupled nonlinear equations which are not, even for subsonic Mach numbers, fully elliptic, but contain hyperbolic partitions. The distributed relaxation approach of Brandt [2, 3] decomposes the system of equations into separable, usually scalar, factors that can be treated with optimal methods. Several years ago, an investigation was started to extend this approach to large-scale applications;

*Computational Modeling and Simulation Branch, Mail Stop 128, NASA Langley Research Center, Hampton, Virginia 23681 (email: j.l.thomas@larc.nasa.gov).

†Institute for Computer Applications in Science and Engineering, Mail Stop 132C, NASA Langley Research Center, Hampton, Virginia 23681 (email: bdiskin@icase.edu). This research was supported by the National Aeronautics and Space Administration under NASA Contract No. NAS1-97046 while the author was in residence at the Institute for Computer Applications in Science and Engineering (ICASE), NASA Langley Research Center, Hampton, Virginia 23681-2199.

‡The Weizmann Institute of Science, Rehovot 76100, Israel (email: achi@wisdom.weizmann.ac.il).

§Williamsburg, Virginia 23185

at that time, several TME demonstrations for incompressible simulations had been completed and Ta'asan had shown promising results for the subsonic Euler equations [18]. Progress has been shown in extending the methodology to viscous compressible flow applications [19] and to compressible Euler equations using a compact differencing scheme [17]. Further incompressible flow applications have been made, including complex geometries [14] and high-Reynolds-number viscous flow in two [20] and three dimensions [13]. The progress and remaining barriers in TME for the equations of fluid dynamics were summarized in [4].

The purpose of this paper is to discuss the general framework expected to be required for large-scale compressible flow applications. The quasi-one-dimensional Euler equations are solved to illustrate the framework. Fully subsonic and supersonic applications, as well as transonic applications with a captured shock, are shown.

2. General Framework. The viscous compressible equations for the time-dependent conservation of mass, momentum, and energy can be written as

$$\partial_t \mathbf{Q} + \mathbf{R} = 0, \quad (2.1)$$

where the conserved variables are $\mathbf{Q} \equiv (\rho, \rho u, \rho v, \rho w, \rho E)^T$, representing the density, momentum vector, and total energy per a unit volume, and $\mathbf{R}(\mathbf{Q})$ is the spatial divergence of a vector function representing convection and viscous and heat transfer effects. In general, the simplest form of the differential equations corresponds to nonconservative equations expressed in primitive variables, here taken as the set composed of velocity, pressure, and internal energy, $\mathbf{q} = (u, v, w, p, \epsilon)^T$. These equations are found readily by transforming the time-dependent conservation equations to time-dependent primitive variable equations. Similarly, a set of nonconservative correction equations can be derived, with a right hand side vector composed of a combination of the conserved residual terms, given as

$$\mathbf{L} \delta \mathbf{q} = -\frac{\partial \mathbf{q}}{\partial \mathbf{Q}} \mathbf{R}. \quad (2.2)$$

In Eq. (2.2), $\frac{\partial \mathbf{q}}{\partial \mathbf{Q}}$ is the Jacobian matrix of the transformation and the correction $\delta \mathbf{q} \equiv \mathbf{q}^{n+1} - \mathbf{q}^n$, where n is an iteration counter. For steady-state equations, the time derivative is dropped. At the discrete level, the right side of the correction equation (2.2) is a combination of conservative-discretization residuals while the left side is the principal linearization of the nonconservative operator.

Note this is not a Newton linearization; only the principal terms in a linearization of \mathbf{R} are retained. The principal terms are those terms that make a major contribution to the residual per a unit change in \mathbf{q} . The principal terms thus generally depend on the scale, or mesh size, of interest. For a *scalar* equation, the discretized highest derivative terms are principal on grids with small enough mesh size h . In deriving the principal linearization for high-Reynolds-number simulations, it is essential to consider both inviscid and viscous scales — the inviscid scales dominate over most of the flow field and the viscous scales are important in the thin viscous layers near bodies and in their wakes. Note that, for a discretized *system* of differential equations, such as $\mathbf{R} = 0$, the principal terms are those that contribute to the principal terms of the *determinant* of the matrix operator $\frac{\partial \mathbf{R}}{\partial \mathbf{q}}$. The coefficients of the principal terms in \mathbf{L} are evaluated from the current approximation.

The principal linearization is applied to the correction equation based on a nonconservative approximation. Thus, we expect the correction to be good away from discontinuities (shocks, slip lines) in the

flow field. It is in these regular (smoothly varying) flow regions that we apply distributed relaxation. The distributed relaxation method replaces $\delta \mathbf{q}$ by $\mathbf{M} \delta \mathbf{w}$ so that the resulting matrix $\mathbf{L} \mathbf{M}$ becomes a diagonal or lower triangular matrix, as

$$\mathbf{L} \mathbf{M} \delta \mathbf{w} = - \frac{\partial \mathbf{q}}{\partial \mathbf{Q}} \mathbf{R}. \quad (2.3)$$

The diagonal elements of $\mathbf{L} \mathbf{M}$ are composed ideally of the separable components of the determinant of the matrix \mathbf{L} and represent the elliptic or hyperbolic factors of the equation. In [3, 8], the $\delta \mathbf{w}$ variables were termed as "ghost variables," because they need not explicitly appear in the calculations.

The distributed relaxation approach yields fast convergence for both steady and unsteady simulations if the constituent scalar diagonal operators in $\mathbf{L} \mathbf{M}$ are solved with fast methods. The approach can be applied to quite general equations; a set of matrices \mathbf{M} has been derived in [3] to provide a convenient lower triangular form for the compressible and incompressible equations of fluid dynamics (including a variable equation of state).

For the compressible Euler equations, the scalar factors constituting the main diagonal of $\mathbf{L} \mathbf{M}$ are convection and full-potential operators. An efficient solver for the former can be based on downstream marching, with additional special procedures for recirculating flows [7, 8, 21]; the latter is a variable type operator, and its solution requires different procedures in subsonic, transonic, and supersonic regions. In deep subsonic regions, the full-potential operator is uniformly elliptic and therefore standard multigrid methods yield optimal efficiency. When the Mach number approaches unity, the operator becomes increasingly anisotropic and, because some smooth characteristic error components cannot be approximated adequately on coarse grids, classical multigrid methods severely degrade. The characteristic components are those components that are much smoother in the characteristic directions than in other directions [4, 11, 10]. In the deep supersonic regions, the full-potential operator is uniformly hyperbolic with the stream direction serving as the time-like direction. In this region, an efficient solver can be obtained with a downstream marching procedure. However, this procedure becomes problematic for the Mach number dropping towards unity, because the Courant number associated with the downstream marching procedure is large. Thus, a special procedure is required to provide an efficient solution for transonic regions. This local procedure [5, 6, 9] is based on piecewise semicoarsening and some rules for adding dissipation at the coarse-grid levels.

Boundaries introduce some additional complexity in distributed relaxation. The determinant of $\mathbf{L} \mathbf{M}$ is usually higher order than the determinant of \mathbf{L} . Thus, as a set of new variables, $\delta \mathbf{w}$ would generally need additional boundary conditions. In relaxation, because the ghost variables can be added in the external part of the domain, it is usually possible to determine suitable boundary conditions for $\delta \mathbf{w}$ that satisfy the original boundary conditions for the primitive variables. Examples are given in [20] in incompressible flow for entering and no-slip boundaries. However, to construct such a remedy may be difficult and/or time-consuming in general. In addition, enforcing these boundary conditions causes the relaxation equations to be coupled near the boundaries, not decoupled as they are in the interior of the domain.

Thus, near boundaries and discontinuities, the general approach [3, 4] is to relax the governing equations directly in terms of primitive variables. Several sweeps of robust (but possibly slowly converging) relaxation, such as Newton-Kacmarcz relaxation, can be made in this region. The additional sweeps will not affect the overall complexity because the number of boundary and/or discontinuity points is usually negligible in comparison with the number of interior points.

This general framework is used below to solve the quasi-one-dimensional Euler equations in fully sub-

sonic, fully supersonic, and transonic (with and without shock) flow regimes. The regular flow regions are relaxed with distributed relaxation. Boundaries and shocks are treated by applying local relaxation — corresponding here to updates through a direct solution of an approximate-Newton linearization of the conservative equations.

In all cases, an FMG-1 algorithm is used; at each level, the equations are solved with an FV(2,1) full approximation scheme (FAS) [2, 20] multigrid cycle. Six levels are used in the cycle wherever possible. The total operation count in the FMG-1 algorithm is equivalent to about 40 residual evaluations. This somewhat excessive operation count is typical for one-dimensional problems, where the number of coarse-grid points is large relative to multidimensional cases. In three-dimensional problems, the expected operation count is about 8 residual evaluations.

3. Quasi-One-Dimensional Equations. The quasi-one-dimensional equations express the conservation of mass, momentum, and total energy as

$$\partial_t(\hat{\mathbf{Q}}) + \hat{\mathbf{R}} = 0, \quad (3.1)$$

where

$$\hat{\mathbf{Q}} \equiv \mathbf{Q}\sigma \equiv (\rho, \rho u, \rho E)^T \sigma, \quad (3.2)$$

$$\hat{\mathbf{R}} \equiv \partial_x(\mathbf{F}\sigma) + \mathbf{S}, \quad (3.3)$$

and $\sigma = \sigma(x)$ is the area term. The flux \mathbf{F} and the source term \mathbf{S} are defined as

$$\mathbf{F} \equiv \begin{pmatrix} \rho u \\ \rho u^2 + p \\ \rho u E + up \end{pmatrix}, \quad (3.4)$$

$$\mathbf{S} \equiv - \begin{pmatrix} 0 \\ p \\ 0 \end{pmatrix} \frac{d\sigma}{dx}. \quad (3.5)$$

The pressure p , internal (thermal) energy ϵ , and sound speed c are related through the equation of state as

$$p = (\gamma - 1)\rho\epsilon, \quad (3.6)$$

$$\epsilon = E - u^2/2, \quad (3.7)$$

$$c^2 = \gamma p / \rho, \quad (3.8)$$

and γ is the ratio of specific heats.

A discrete conservative upwind-biased differencing approximation to $\hat{\mathbf{R}}$ can be defined for first- or second-order accuracy as

$$\begin{aligned} \hat{\mathbf{R}}_j &= \frac{1}{h} [(\mathbf{F}\sigma)_{j+\frac{1}{2}} - (\mathbf{F}\sigma)_{j-\frac{1}{2}}] \\ &\quad - (0, p_j, 0)^T [\sigma_{j+\frac{1}{2}} - \sigma_{j-\frac{1}{2}}]. \end{aligned} \quad (3.9)$$

Here, a finite-volume discretization is used, where subscripts $j + \frac{1}{2}$ and $j - \frac{1}{2}$ denote the right and left interfaces, respectively, of the cell centered at location j and the cell spacing in the x -direction is h . The flux-differencing splitting of Roe [15] is used to construct the interface flux $\mathbf{F}_{j+\frac{1}{2}}$; pertinent details are described in appendix A. We consider only first- or second-order accuracy and do not differentiate between average and pointwise values of \mathbf{Q} . The area distribution is defined as $\sigma(x) = 1 - 0.8x(1 - x)$. For all of the results presented below, we overprescribe the boundary values from the exact solution of the differential problem at the cell centers that lie outside of the domain $0 \leq x \leq 1$.

4. Relaxation Schemes. Several schemes are considered below for relaxation of the steady-state equations

$$\widehat{\mathbf{R}}_j = 0. \quad (4.1)$$

The schemes are all written in delta form, so that the correction to the solution is solved at each iteration, denoted as $\delta\mathbf{Q} \equiv \mathbf{Q}^{n+1} - \mathbf{Q}^n$.

4.1. Conservative Relaxation Scheme. The exact Newton linearization of the discrete conservative equations generally leads to an overly complicated linear system to solve. In practice, a quasi-Newton (approximate) linearization is used to reduce the algebraic complexity of the construction and/or the bandwidth of the resulting linear system. For the purpose of constructing a conservative relaxation scheme, an approximate but conservative linearization of the operator (3.9) can be written as

$$[\delta_x^- \mathbf{A}^+ + \delta_x^+ \mathbf{A}^-](\mathbf{Q}). \quad (4.2)$$

The operators δ_x^- and δ_x^+ denote backward and forward first-order-accurate difference operators, respectively, and \mathbf{A}^+ and \mathbf{A}^- denote the positive and negative eigenvalue contributions to the similarity matrices (see appendix A and [12] for references).

The conservative relaxation update $\delta\mathbf{Q}$ is computed from

$$[\delta_x^- \mathbf{A}^+ + \delta_x^+ \mathbf{A}^-](\delta\mathbf{Q}) = -\frac{1}{\sigma_j} \widehat{\mathbf{R}}_j. \quad (4.3)$$

The residuals in the right side of Eq. (4.3) are computed for the target discretization (4.1). The relaxation procedure requires a tridiagonal equation to be directly solved:

$$(-\mathbf{A}_{j-1}^+, |\mathbf{A}|_j, \mathbf{A}_{j+1}^-)(\delta\mathbf{Q}) = -\frac{h}{\sigma_j} \widehat{\mathbf{R}}_j. \quad (4.4)$$

Barth [1] analyzed this relaxation with fixed-point analysis and showed the relaxation is nearly as good as a full Newton iteration. An underrelaxation parameter, e.g., a pseudo-time step, can be introduced in the relaxation scheme to improve robustness and stability. Extensive computations made during the course of this investigation verified that this relaxation method can be used throughout the domain, including shocks and boundaries. In the general framework described and used in this paper, this relaxation is applied only locally to reduce residuals near boundaries and shocks and to solve the coarsest grid equation. In multidimensional case, any stable procedure converging for the primitive-variable conservative equations

(4.1) (e.g., pseudo-time marching relaxation) can be applied for local relaxation. The large operation count per point required for convergence in this procedure does not affect the overall complexity of the algorithm, because the number of grid points in the local-relaxation regions is assumed to be negligible in comparison with the total number of grid points.

4.2. Nonconservative Relaxation Scheme. A nonconservative relaxation scheme is derived from a conservative scheme, Eq. (4.3), with the assumption that the Jacobian matrices are locally constant,

$$[\mathbf{A}^+ \delta_x^- + \mathbf{A}^- \delta_x^+](\delta \mathbf{Q}) = -\frac{1}{\sigma_j} \hat{\mathbf{R}}_j. \quad (4.5)$$

This formulation is expected to be a good approximation to Eq. (4.3), except near discontinuities. The corresponding tridiagonal equation is

$$(-\mathbf{A}_j^+, |\mathbf{A}|_j, \mathbf{A}_j^-)(\delta \mathbf{Q}) = -\frac{h}{\sigma_j} \hat{\mathbf{R}}_j. \quad (4.6)$$

Subtracting the two tridiagonal equations, (4.4) and (4.6) yields

$$(-\mathbf{A}_{j-1}^+ + \mathbf{A}_j^+, 0, \mathbf{A}_{j+1}^- - \mathbf{A}_j^-)(\delta \mathbf{Q}) = 0, \quad (4.7)$$

where the coefficients $-\mathbf{A}_{j-1}^+ + \mathbf{A}_j^+$ and $\mathbf{A}_{j+1}^- - \mathbf{A}_j^-$ are $O(h)$ small on sufficiently fine meshes in regular flow regions. Near shocks, the nonconservative linearization used in Eq. (4.5) does not satisfy an order property and the nonconservative relaxation scheme would not be effective. These expectations were confirmed through computations with both the conservative and nonconservative relaxation schemes, where update Eqs. (4.4) and (4.6) were solved precisely. Barth [1] analyzed a similar nonconservative relaxation scheme with fixed-point analysis and showed poor performance of the nonconservative scheme for a flow with a shock.

4.3. Distributed Relaxation. Away from boundaries and shocks, the linear update scheme Eq. (4.5) is relaxed with distributed relaxation. Transforming the corrections in Eq. (4.5) to primitive variables $\mathbf{q} = (u, p, \epsilon)^T$ gives

$$[\bar{\mathbf{A}}^+ \delta_x^- + \bar{\mathbf{A}}^- \delta_x^+](\delta \mathbf{q}) = -\left(\frac{\partial \mathbf{q}}{\partial \mathbf{Q}}\right)_j \frac{1}{\sigma_j} \hat{\mathbf{R}}_j, \quad (4.8)$$

with a right-side vector composed of a combination of the conserved residual terms. The Jacobian matrices are related through a similarity transformation to the conservative Jacobians:

$$\bar{\mathbf{A}} = \frac{\partial \mathbf{q}}{\partial \mathbf{Q}} \mathbf{A} \frac{\partial \mathbf{Q}}{\partial \mathbf{q}}. \quad (4.9)$$

Alternately, by definition, the primitive variable correction equation is

$$\mathbf{L} \delta \mathbf{q} = -\bar{\mathbf{r}}_j, \quad (4.10)$$

where

$$\bar{r}_j = \left(\frac{\partial \mathbf{q}}{\partial \mathbf{Q}} \right)_j \frac{1}{\sigma_j} \hat{\mathbf{R}}_j. \quad (4.11)$$

The elements of the matrix operator \mathbf{L} are given in appendix B.

As follows from Appendices A and B, the determinant of \mathbf{L} for $(u > 0)$ in deep subsonic or supersonic regions is

$$\det(\mathbf{L}) = [(u^2 - c^2) \delta_{xx}] u \delta_x^-, \quad (4.12)$$

where

$$\delta_{xx} \equiv \begin{cases} \delta_x^- \delta_x^+ & \text{for fully subsonic flow,} \\ \delta_x^- \delta_x^- & \text{for fully supersonic flow.} \end{cases} \quad (4.13)$$

The first term in Eq. (4.12) represents an approximation to the full-potential operator and the second term represents an upwind approximation for the convection of entropy. In subsonic flow, δ_{xx} is a central discretization associated with the ellipticity of the full-potential operator. In fully supersonic flow, δ_{xx} is a one-sided or upwind-biased approximation in accordance with the hyperbolic nature of the full-potential operator. For first-order upwind differencing, the full-potential factor is a 3-point operator; for second-order upwind-biased differencing, the factor is a 7-point operator (see appendix B).

In this one-dimensional case, the first two equations in the matrix operator \mathbf{L} are uncoupled from the third. Thus we need only consider distributed relaxation of the first two equations; the third equation can be solved for $\delta\epsilon$ in its primitive variable form once δu and δp are found from distributed relaxation. Denoting the upper 2×2 block of \mathbf{L} as $\bar{\mathbf{L}}$, an obvious choice for $\bar{\mathbf{M}}$ is the matrix of cofactors of $\bar{\mathbf{L}}$, which gives a diagonal matrix for $\bar{\mathbf{L}}\bar{\mathbf{M}}$ with the full-potential factors along the diagonal, i.e.,

$$\bar{\mathbf{L}}\bar{\mathbf{M}} = \begin{pmatrix} (u^2 - c^2) \delta_{xx} & 0 \\ 0 & (u^2 - c^2) \delta_{xx} \end{pmatrix}. \quad (4.14)$$

4.4. Boundary Treatment. As pointed out by Sidilkover [17], there is a connection between distributed relaxation and the characteristic variables. For subsonic flow, a Jacobi update to the operators in $\bar{\mathbf{L}}\bar{\mathbf{M}}$ is equivalent to a Kacmarcz relaxation of the characteristic equations, cast in terms of a characteristic combination of corrections as

$$\begin{pmatrix} (u + c) \delta_x^- (\rho c \delta u + \delta p) \\ (u - c) \delta_x^+ (\rho c \delta u - \delta p) \end{pmatrix} = - \begin{pmatrix} \rho c \bar{r}_1 + \bar{r}_2 \\ \rho c \bar{r}_1 - \bar{r}_2 \end{pmatrix}_j. \quad (4.15)$$

With first-order differencing, an equal and opposite correction to the downstream propagating characteristic variable $\rho c \delta u + \delta p$ is sent in Kacmarcz relaxation of the first equation to the local cell j and to the upstream cell $j - 1$; the correction to cell j is exactly one half of that found from a point Jacobi relaxation of the corresponding characteristic equation. Likewise, an equal and opposite correction to the upstream propagating characteristic variable $\rho c \delta u - \delta p$ is sent in Kacmarcz relaxation of the second equation to the local cell j and to the downstream cell $j + 1$. With a local update of the solution at each point, the smoothing

TABLE 1

The discretization errors in p at convergence and the relative L_1 -norm errors after the FMG-1 algorithm for fully subsonic flow.

h	$\ e_d\ : p$	$\frac{\ e_s\ - \ e_d\ }{\ e_d\ } : p$
1/32	0.2654×10^{-3}	< 0.01
1/64	0.6341×10^{-4}	< 0.01
1/128	0.1547×10^{-4}	< 0.01
1/256	0.3817×10^{-5}	< 0.01

rate should be equivalent to Gauss-Seidel relaxation of the standard 3-point Laplacian operator. However, the relaxation at cells adjacent to the boundary is inconsistent with the boundary conditions of the original problem; for example, characteristic boundary conditions would prescribe $\rho c \delta u + \delta p$ and $\rho c \delta u - \delta p$ as zero at the upstream and downstream boundaries, respectively.

This example demonstrates the general result mentioned earlier: that distributed relaxation needs to be modified near the boundaries. A simple boundary specification for the ghost variable $\delta \mathbf{w} = (\delta w_1, \delta w_2)^T$ can be found in this case; enforcing a Neumann condition on δw_1 (δw_2) and a Dirichlet condition on δw_2 (δw_1) at inflow (outflow) in subsonic relaxation is consistent with characteristic boundary conditions in terms of primitive variables. We instead use the more general formulation and apply another local conservative relaxation procedure at the boundary points to reduce the residuals. Distributed relaxation is then applied in the interior with simple Dirichlet conditions for the ghost variables $\delta \mathbf{w}$.

4.5. Relaxation Sequence. The general solution procedure was to reduce the local residuals at least two orders of magnitude at the inflow boundary, the outflow boundary, and then at the shock region — both before and after sweeping the entire domain with distributed relaxation. The local conservative relaxation is made over the first two cells adjacent to the boundary. In the shock region, the local conservative relaxation was applied to nine cells centered on the upstream (supersonic) side of the shock. A pseudo-time step corresponding to a Courant number of 100 was used as an underrelaxation factor in the local conservative relaxations; otherwise purely steady-state equations were relaxed. In distributed relaxation, the variables $(\delta w_1, \delta w_2)^T$ were explicitly used in the implementation; they were first relaxed over the interior cells, then distributions to $(\delta u, \delta p)^T$ were made, and then the corrections to $\delta \epsilon$ were computed. As a check, single-grid computations verified that the convergence of the error per relaxation of subsonic equations (4.1) with first-order differencing was identical to that found with a Gauss-Seidel relaxation of the one-dimensional 3-point Laplacian operator with Neumann boundary conditions applied at one end of the domain.

5. Computational Results. Computational results are shown in this section for fully subsonic, fully supersonic, and transonic flow with and without a shock. The Mach number distribution with second-order accurate discretization on a grid of 257 points is shown in Fig. 1 for fully subsonic, fully supersonic, and transonic flow with a shock; the shock location is specified at $x = 0.75$. There is no limiting applied in the transonic cases so there are some oscillations at the shock. In this one-dimensional case, the solution can easily be repaired by using an essentially nonoscillatory (ENO) [16] approach (see appendix C) but the emphasis of this work is on the solution procedure and not on the steady-state results.

5.1. Fully Subsonic Flow. The smoothing rate of distributed relaxation for the primitive variable equations is expected to be equal to the worst among the smoothing rates obtained in relaxation of the scalar factors of the determinant of \mathbf{L} , in our case convection and the full-potential factor. With the full-

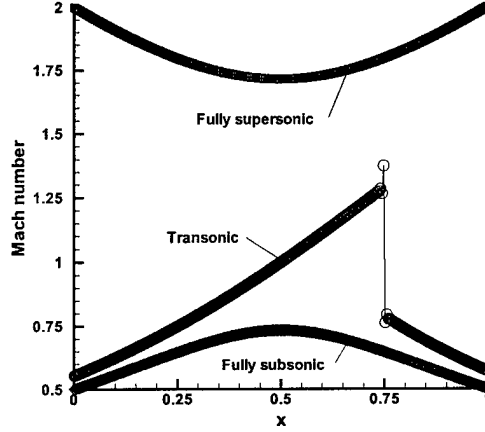


FIG. 1. Mach number distribution computed without limiting on a grid of 257 points for fully subsonic, fully supersonic, and transonic flow with a shock at $x = 0.75$.

potential operator *relaxed* (Gauss-Seidel) and the convection operator *solved* by downstream marching from the inflow boundary, the convergence rate of the multigrid cycle per relaxation sweep for the first-order accurate discretization should be close to the smoothing factor, 0.447, of Gauss-Seidel relaxation for the one-dimensional 3-point Laplacian operator.

Defect correction is often used in the solution of higher order implicit discretizations to reduce the arithmetic operation count while retaining the target accuracy. One seemingly possible implementation of defect correction is to use first-order accurate discretizations for the convection operators in \mathbf{L} . The corresponding distribution matrix \mathbf{M} consists of the first-order operators as well. This implementation, however, is not a good idea for obtaining good *smoothing* rates, because *in terms of high-frequency components*, a low-order operator and a corresponding high-order operator do not necessarily approximate each other well. Indeed, this implementation caused a slowdown in the convergence, and the smoothing rate corresponding to that of the Laplace equation was not attained.

To illustrate this phenomenon, consider the Laplacian operator alone. The elliptic operator $\delta_{xx}(w_j)$ arising from differencing the primitive variable equations with the second-order upwind-biased operator used here is a 7-point operator (see appendix B). Corrections $(\delta w)_j$ to the current approximate solutions w_j computed in Gauss-Seidel defect-correction relaxation with the 3-point Laplacian as a left-side (driver) operator can be found from

$$\frac{1}{h^2}[(\delta w)_{j-1} - 2(\delta w)_j] = -\delta_{xx}(w_j). \quad (5.1)$$

The smoothing factor, computed with local mode analysis, of this defect-correction relaxation (5.1) is $g_s = 0.525$, which is substantially smaller than the convergence rate per distributed relaxation of 0.9 observed with a multigrid FV(2,1) cycle applied to Eq. (4.10). The smoothing factor of distributed relaxation for Eq. (4.10) is computed by using local mode analysis as a norm of the matrix $\hat{\mathbf{G}}$, defined as

$$\hat{\mathbf{G}} = \mathbf{I} - (1 - g_s)(\hat{\mathbf{M}}_d)^{-1}\hat{\mathbf{M}}_l, \quad (5.2)$$

TABLE 2

The discretization errors in p at convergence and the relative L_1 -norm errors after the FMG-1 algorithm for fully supersonic flow.

h	$\ e_d\ : p$	$\frac{\ e_t\ - \ e_d\ }{\ e_d\ } : p$
1/32	0.8890×10^{-4}	< 0.01
1/64	0.2151×10^{-4}	0.02
1/128	0.5278×10^{-5}	< 0.01
1/256	0.1306×10^{-5}	< 0.01

where matrix symbols associated with distribution matrices for target (second-order) and driver (first-order) operators are denoted $\widehat{\mathbf{M}}_t$ and $\widehat{\mathbf{M}}_d$, respectively. The calculated smoothing factor is 0.752, appreciably greater than the expected value of 0.525. The increased smoothing factor is explained by the fact that $(\widehat{\mathbf{M}}_d)^{-1}\widehat{\mathbf{M}}_t$ is far different from the identity matrix.

With corrections distributed by the second-order distribution matrix operator ($\mathbf{M}_d = \mathbf{M}_t$), the smoothing factor of distributed relaxation for Eq. (4.10) should be identical to that for relaxation of the Laplacian equation. Implementing the defect-correction relaxation (5.1) of the Laplacian equation but distributing corrections with the second-order distribution yielded an FV(2,1) cycle convergence rate per smoothing of 0.51 — close to 0.525 predicted by the mode analysis of the defect-correction relaxation (5.1).

Results for an FMG-1 algorithm, denoting a full multigrid algorithm with one FV(2,1) cycle at each level, are shown for fully subsonic flow in Table 1. All of the norms used in this and the following tables are L_1 -norms. The discretization error in pressure is defined pointwise as $e_d \equiv \bar{p}_j - p(x_j)^{\text{exact}}$, where $p(x)^{\text{exact}}$ is the steady-state solution of Eq. (3.1) and \bar{p}_j is the discrete solution of Eq. (4.1). A second-order spatial convergence in the L_1 -norm of e_d is evident. The total error in pressure is defined as $e_t \equiv p(x_j)^{\text{exact}} - p_j$, where p_j is the approximate solution obtained in the FMG-1 algorithm. Small relative difference between L_1 -norms of the total and discretization errors (see Table 1) indicates that optimal efficiency has been attained. The asymptotic convergence rate of the FV(2,1) cycle was 0.50–0.52 per relaxation for any of the four grids.

5.2. Fully Supersonic Flow. In fully supersonic flow, it is generally possible to construct marching methods to solve the full-potential equation. For first-order differencing, the one-sided operator can easily be solved over the domain. For the second-order operator considered here, the defect-correction relaxation with the first-order upwind driver can be defined as

$$\frac{1}{h^2}[(\delta w)_{j-2} - 2(\delta w)_{j-1} + (\delta w)_j] = -\delta_{xx}(w_j). \quad (5.3)$$

This scheme can be solved by marching but, unfortunately, its amplification factor is larger than 1 for some error components. A suitable full-potential driver operator to replace the left-side operator of Eq. (5.3) can be found in the form

$$[\delta_x^- + h\alpha\delta_x^-\delta_x^-]^2, \quad (5.4)$$

where the backward difference operator is defined to be first-order in the above expression. This is a 5-point operator that can be solved by marching. The maximum amplification factor of the supersonic defect-correction relaxation with the driver (5.4) and $\alpha = 0.23$ is 0.55. With the second-order distribution operator,

TABLE 3

The discretization errors in p at convergence and the relative L_1 -norm errors after the FMG-1 algorithm for transonic flow without a shock.

h	$\ e_d\ : p$	$\frac{\ e_t\ - \ e_d\ }{\ e_d\ } : p$
1/32	0.1075×10^{-3}	0.05
1/64	0.2666×10^{-4}	0.09
1/128	0.6635×10^{-5}	0.03
1/256	0.1655×10^{-5}	0.11

TABLE 4

The discretization errors in p at convergence and the relative L_1 -norm errors after the FMG-1 algorithm for transonic flow with a shock.

h	$\ e_d\ : p$	$\frac{\ e_t\ - \ e_d\ }{\ e_d\ } : p$
1/32	0.4396×10^{-2}	<0.01
1/64	0.2218×10^{-2}	0.015
1/128	0.1111×10^{-2}	0.014
1/256	0.5558×10^{-3}	<0.01

computations for the fully supersonic flow corresponding to Mach 2 at inflow converged asymptotically at this rate.

Results for the FMG-1 algorithm are shown in Table 2. The L_1 -norm of the discretization error in pressure shows the expected second-order spatial convergence. Optimal efficiency is attained with the FMG-1 algorithm. Here, the performance of the single-grid iteration at each level is the same as an FV(2,1) cycle, because the full-potential factor is being solved (rather than just smoothed) by marching. The asymptotic convergence rate per relaxation was 0.53–0.56 for any of the four grids.

5.3. Transonic Flows. Results for the FMG-1 algorithm are shown for a smooth transonic flow in Table 3. The L_1 -norm of the discretization error in pressure shows the expected second-order spatial convergence. The relative deviations of the L_1 -norm of the total errors from the L_1 -norm of the discretization errors are increased from the fully subsonic or fully supersonic levels but still exhibit optimal performance. The asymptotic convergence rate per relaxation was 0.52–0.56 for any of the four grids.

Results for the FMG-1 algorithm are shown for the transonic flow with a shock in Table 4. The L_1 -norm of the discretization error in pressure shows a first-order spatial convergence, because there is no limiting of the interpolation at the shock; i.e., maximum local errors occur at the shock and do not diminish with grid refinement. The relative deviations of the L_1 -norm of the total error with the FMG-1 algorithm from the L_1 -norm of the discretization error again exhibit optimal performance. The average convergence rate per relaxation over 10 cycles varied from 0.35 on the coarsest mesh to 0.51 on the finest mesh. Computations for this case with ENO differencing are presented in appendix C and show a similar performance with a monotone solution behavior in the shock region.

6. Concluding Remarks. A general multigrid framework for obtaining textbook efficiency to solutions of the compressible Euler and Navier-Stokes equations in conservation law form has been discussed. The general methodology relies on a distributed relaxation procedure to reduce errors in regular (smoothly varying) flow regions; separate and distinct treatments for each of the factors (elliptic and/or hyperbolic) are

used to attain optimal reductions of errors. Near the boundaries and near shocks, additional local relaxations of the conservative equations are necessary. Example calculations are made for the quasi-one-dimensional Euler equations for situations with fully subsonic and fully supersonic flow, as well as transonic flows with and without a shock. All of the calculations showed that the FMG-1 algorithm provides a very accurate approximation of the exact solution.

REFERENCES

- [1] T. J. BARTH, *Analysis of implicit local linearization techniques for upwind and TVD algorithms*, 1987. AIAA Paper 87-0595.
- [2] A. BRANDT, *Guide to multigrid development*, in Multigrid Methods, W. Hackbusch and U. Trottenberg, eds., Lecture Notes in Math. 960, Springer-Verlag, Berlin, 1982.
- [3] —, *Multigrid techniques: 1984 guide with applications to fluid dynamics*, in Lecture Notes for the Computational Fluid Dynamics, Lecture Series at the Von-Karman Institute for Fluid Dynamics, The Weizmann Institute of Science, Rehovot, Israel, 1984. ISBN-3-88457-081-1, GMD-Studien Nr. 85, Available from GMD-AIW, Postfach 1316, D-53731, St. Augustin 1, Germany. Also available from Secretary, Department of Mathematics, University of Colorado at Denver, CO 80204-5300.
- [4] —, *Barriers to achieving textbook multigrid efficiency in CFD*, ICASE Interim Report 32, NASA CR-1998-207647, April 1998. Updated version available as Gauss Center Report WI/GC-10 at The Weizmann Institute of Science, Rehovot, Israel, December 1998.
- [5] A. BRANDT AND B. DISKIN, *Multigrid solvers for the non-aligned sonic flow: The constant coefficient case*, Computers and Fluids, 28 (1999), pp. 511–549. Also Gauss Center Report WI/GC-8 at The Weizmann Institute of Science, Rehovot, Israel, October 1997.
- [6] —, *Multigrid solvers for nonaligned sonic flows*, SIAM J. Sci. Comp., 21 (2000), pp. 473–501.
- [7] A. BRANDT AND I. YAVNEH, *On multigrid solution of high-Reynolds incompressible entering flow*, J. Comput. Phys., 101 (1992), pp. 151–164.
- [8] —, *Accelerated multigrid convergence and high-Reynolds recirculating flows*, SIAM J. Sci. Comp., 14 (1993), pp. 607–626.
- [9] B. DISKIN, *Efficient Multigrid Solvers for the Linearized Transonic Full Potential Equation*, PhD thesis, The Weizmann Institute of Science, 1998.
- [10] B. DISKIN AND J. L. THOMAS, *Half-space analysis of the defect-correction method for Fromm discretization of convection*. To appear in SIAM J. Scient. Comp.
- [11] —, *Solving upwind-biased discretizations: Defect-correction iterations*, ICASE Report 99-14, NASA CR-1999-209106, March 1999.
- [12] C. HIRSCH, *Numerical computation of internal and external flows*, vol. 2, Computational methods for inviscid and viscous flows, John Wiley & Sons, Inc., 605 Third Avenue, New York, NY 10158-0012, USA, 1988.
- [13] R. S. MONTERO AND I. M. LLORENTE, *Robust multigrid algorithms for the incompressible Navier-Stokes equations*, ICASE Report 2000-27, NASA CR-2000-210126, May 2000.
- [14] T. W. ROBERTS AND R. C. SWANSON, *Extending ideally converging multigrid methods to airfoil flows*, AIAA Paper 99-3337, 14th AIAA CFD meeting, Norfolk, VA, June-July 1999.
- [15] P. L. ROE, *Approximate Riemann solvers, parameter vectors, and difference schemes*, J. Comp. Phys., 43 (1981), pp. 357–72.

- [16] C. W. SHU, *Essentially nonoscillatory and weighted essentially nonoscillatory schemes for hyperbolic conservation laws*, ICASE Report 97-65, NASA CR-97-206253, November 1997.
- [17] D. SIDILKOVER, *Some approaches toward constructing optimally efficient multigrid solvers for the inviscid flow equations*, Computers and Fluids, 28 (1999), pp. 551–571.
- [18] S. TA'ASAN, *Canonical-variables multigrid method for steady-state Euler equations*, ICASE Report 94-14, NASA CR-194888, 1994.
- [19] J. L. THOMAS, B. DISKIN, AND A. BRANDT, *Distributed relaxation multigrid and defect correction applied to the compressible Navier-Stokes equations*, AIAA Paper 99-3334, 14th Computational Fluid Dynamics Conference, Norfolk, VA, July 1999.
- [20] —, *Textbook multigrid efficiency for the incompressible Navier-Stokes equations: High Reynolds number wakes and boundary layers*, ICASE Report 99-51, NASA CR-1999-209831, December 1999. To appear in *Computers and Fluids*.
- [21] I. YAVNEH, C. VENNER, AND A. BRANDT, *Fast multigrid solution of the advection problem with closed characteristics*, SIAM J. Sci. Comp., 19 (1998), pp. 111–125.

Appendix A. Conservative Fluxes.

The fluxes are constructed by using the flux-difference splitting of Roe [15] and are given as

$$\mathbf{F}_{j+\frac{1}{2}} = \frac{1}{2}[\mathbf{F}(\mathbf{Q}_R) + \mathbf{F}(\mathbf{Q}_L) - |\tilde{\mathbf{A}}|(\mathbf{Q}_R - \mathbf{Q}_L)] \quad (\text{A.1})$$

where $\hat{\mathbf{A}} \equiv \partial \mathbf{F} / \partial \mathbf{Q}$ is evaluated with a specific average of the left and right states, \mathbf{Q}_L and \mathbf{Q}_R , in order to exactly satisfy the jump conditions for a shock [15]. The left and right states are constructed for first-order accuracy as

$$\mathbf{Q}_L = \mathbf{Q}_j, \quad (\text{A.2})$$

$$\mathbf{Q}_R = \mathbf{Q}_{j+1}, \quad (\text{A.3})$$

and for second-order accuracy with Fromm's discretization as

$$\mathbf{Q}_L = \mathbf{Q}_j + \frac{1}{4}(\mathbf{Q}_{j+1} - \mathbf{Q}_{j-1}), \quad (\text{A.4})$$

$$\mathbf{Q}_R = \mathbf{Q}_{j+1} - \frac{1}{4}(\mathbf{Q}_j - \mathbf{Q}_{j+2}). \quad (\text{A.5})$$

The dissipation matrix $|\tilde{\mathbf{A}}| \equiv \mathbf{T} |\tilde{\Lambda}| \mathbf{T}^{-1}$ where $\mathbf{T}, \mathbf{T}^{-1}$ are diagonalizing matrices, the matrix of eigenvalues is

$$\Lambda \equiv \begin{bmatrix} \lambda_1 & 0 & 0 \\ 0 & \lambda_2 & 0 \\ 0 & 0 & \lambda_3 \end{bmatrix}, \quad (\text{A.6})$$

and

$$(\lambda_1, \lambda_2, \lambda_3)^T = (u + c, u - c, u)^T. \quad (\text{A.7})$$

The tilde superscript denotes that the eigenvalues are limited away from zero as,

$$|\tilde{\lambda}_i| \equiv \begin{cases} |\lambda_i| & \text{if } |\lambda_i| \geq \tilde{\epsilon}, \\ (\lambda_i^2 + (\tilde{\epsilon})^2)/(2\tilde{\epsilon}) & \text{otherwise,} \end{cases} \quad (\text{A.8})$$

mainly to prevent expansion shocks at sonic points for the first-order discretization accuracy, but also to make a smooth transition through the sonic point for the full-potential operator. The value $\tilde{\epsilon}$ is taken as $\beta \max\{|\lambda_1|, |\lambda_2|, |\lambda_3|\}$. This “entropy fix” is not optimal in any sense, as larger β values for sonic points are required for the first order scheme on coarser grids. The value of β was nominally set at 0.1 and was arbitrarily increased to 0.2 for grids of 9 points or less in the implicit first-order Jacobian matrices.

Appendix B. Distribution Matrices.

The coefficient matrices $\bar{\mathbf{A}}^\pm$ are defined as the positive and negative eigenvalue contributions to $\bar{\mathbf{A}}$, where

$$\lambda_i^\pm \equiv (\lambda_i \pm |\tilde{\lambda}_i|)/2 \quad (\text{B.1})$$

and $\bar{\mathbf{A}}$ is written in terms of its eigenvalues, $\bar{\mathbf{A}}(\lambda_1, \lambda_2, \lambda_3)$, as

$$\begin{bmatrix} \frac{1}{2}(\lambda_1 + \lambda_2) & \frac{1}{2\rho c}(\lambda_1 - \lambda_2) & 0 \\ \frac{\rho c}{2}(\lambda_1 - \lambda_2) & \frac{1}{2}(\lambda_1 + \lambda_2) & 0 \\ \frac{c}{2\gamma}(\lambda_1 - \lambda_2) & \frac{1}{2\rho\gamma}(\lambda_1 + \lambda_2 - 2\lambda_3) & \lambda_3 \end{bmatrix}. \quad (\text{B.2})$$

The upper 2×2 block of $\mathbf{L} \equiv \bar{\mathbf{A}}^+ \delta_x^- + \bar{\mathbf{A}}^- \delta_x^+$ can be written as

$$\bar{\mathbf{L}} = \begin{bmatrix} t_1 & \frac{1}{\rho c}(t_2) \\ \rho c(t_2) & t_1 \end{bmatrix}. \quad (\text{B.3})$$

and the corresponding matrix of cofactors is

$$\bar{\mathbf{M}} = \begin{bmatrix} t_1 & -\frac{1}{\rho c}(t_2) \\ -\rho c(t_2) & t_1 \end{bmatrix}. \quad (\text{B.4})$$

where

$$t_1 = \frac{1}{2} [(\lambda_1^+ + \lambda_2^+) \delta_x^- + (\lambda_1^- + \lambda_2^-) \delta_x^+], \quad (\text{B.5})$$

$$t_2 = \frac{1}{2} [(\lambda_1^+ - \lambda_2^+) \delta_x^- + (\lambda_1^- - \lambda_2^-) \delta_x^+]. \quad (\text{B.6})$$

The determinant of $\bar{\mathbf{L}}$ is

$$\begin{aligned} t_1^2 - t_2^2 &= (\lambda_1^+ \lambda_2^+) \delta_x^- \delta_x^- \\ &\quad + (\lambda_1^+ \lambda_2^- + \lambda_1^- \lambda_2^+) \delta_x^- \delta_x^+ \\ &\quad + (\lambda_1^- \lambda_2^-) \delta_x^+ \delta_x^+ \end{aligned} \quad (\text{B.7})$$

TABLE 5

The discretization errors in p with ENO differencing at convergence and the relative L_1 -norm errors after the FMG-1 algorithm for transonic flow with a shock.

h	$\ e_d\ : p$	$\frac{\ e_e\ - \ e_d\ }{\ e_d\ } : p$
1/32	0.3597×10^{-3}	< 0.01
1/64	0.9711×10^{-4}	0.01
1/128	0.5133×10^{-4}	0.07
1/256	0.2665×10^{-5}	0.13

The operators for second-order upwind-biased differencing are defined as

$$\delta_x^- \delta_x^+(w_j) = \frac{1}{16h^2}(-w_{j-3} + 2w_{j-2} + 17w_{j-1} - 36w_j + 17w_{j+1} + 2w_{j+2} - w_{j+3}), \quad (\text{B.8})$$

$$\delta_x^- \delta_x^-(w_j) = \frac{1}{16h^2}(w_{j-4} - 10w_{j-3} + 31w_{j-2} - 28w_{j-1} - w_j + 6w_{j+1} + w_{j+2}). \quad (\text{B.9})$$

Appendix C. Transonic Shock — ENO Differencing.

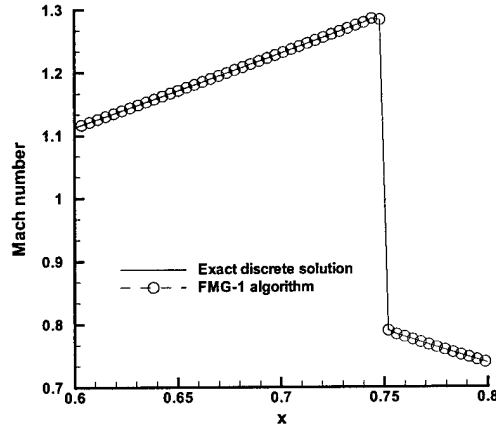


FIG. 2. Mach number distribution near the shock computed with the FMG-1 algorithm compared to the exact discrete solution ($h = 1/256$).

Uniform application of the upwind-biased interpolations for state variables of appendix A (Fromm's scheme) leads to oscillations at the shock. These oscillations can be eliminated by a limiting procedure to reduce locally the order of approximation in the region of the shock. Here, an ENO approach [16] is used to prevent state-variable interpolations from crossing the shock. At the shock interface, the left (right) state variables, $Q_L(Q_R)$, are found by one-sided second-order extrapolation; at the first interface upstream (downstream) of the shock, the state variables, $Q_L(Q_R)$, are found by second-order central averaging.

Fig. 2 presents the Mach number distribution in the region of the shock and shows a nonoscillatory behavior with a one-point representation of the shock. The averaged convergence rate per relaxation obtained in the FV(2,1) cycle was ranged from 0.36 to 0.44 for different target grids. The discretization errors and relative deviations of the L_1 -norm of the total error with the FMG-1 algorithm are shown in Table 5; comparison with Table 4 shows that the ENO discretization errors are smaller than the discretization errors of the unlimited interpolations, although first-order behavior is still found. In both situations, for this one-dimensional case, second-order accuracy is attained if the L_1 -norm is restricted to regions either far upstream or far downstream of the shock. Although not shown, we note that for this case, uniform second-order accuracy can be found with the ENO procedure above if the entropy fix is dropped at the shock; the shock jump is then reconstructed identically, and a zero-point shock is recovered. The focus of this investigation is on convergence, and both Fig. 2 and Table 5 indicate optimal efficiency has been attained with the FMG-1 algorithm.